Mol. Cells *29*, 175-183, February 28, 2010
DOI/10.1007/s10059-010-0011-5

Molecules and Cells

Silencing of NbCEP1 Encoding a Chloroplast Envelope Protein Containing 15 Leucine-Rich-Repeats Disrupts Chloroplast Biogenesis in *Nicotiana benthamiana*

Young Jeon[1], A-Reum Hwang[1,3], Inhwan Hwang[2], and Hyun-Sook Pai[1,*]

We characterized the physiological functions of *Nicotiana benthamiana* Chloroplast Envelope Protein 1 (NbCEP1) in *Nicotiana benthamiana*. NbCEP1 contains a chloroplast transit peptide and a single transmembrane domain at the N terminus, and most of its protein coding region is comprised of 15 leucine-rich-repeats (LRRs). The *NbCEP1* gene is expressed in both aerial and underground plant tissues, and is induced by light. A GFP fusion protein of full length NbCEP1 was targeted to the chloroplast envelope and co-localized with OEP7:RFP, a marker protein for the chloroplast envelope. A fusion protein consisting of GFP and the NbCEP1 transit peptide mainly localized in the chloroplast stroma. Reduction of *NbCEP1* expression by virus-induced gene silencing resulted in a leaf yellowing phenotype without much affecting overall plant growth. At the cellular level, depletion of NbCEP1 severely influenced chloroplast development, reducing both the number and size of the chloroplasts. Interestingly, mitochondrial development was also impaired, possibly an indirect effect of chloroplast ablation. A deficiency in NbCEP1 activity decreased the chlorophyll and carotenoid levels. Our results suggest that NbCEP1 plays a critical function, possibly through protein-protein interactions mediated by its LRRs, in chloroplast development in *N. benthamiana.*

INTRODUCTION

There are >2,000 proteins that contain leucine-rich-repeats (LRRs) from viruses to eukaryotes, including receptor kinases, hormone receptors, cell adhesion molecules and diverse enzymes (Enkhbayar et al., 2003; Kobe and Kajava, 2001). LRRs are highly variable in the number of repeats (2 to 45), their lengths (20 to 30 amino acids), and their conserved sequences, but the motif invariably seems to be involved in protein-protein interactions. The structure of LRRs has been determined in a number of proteins with diverse functions, including ribonuclease inhibitor (RI), RanGAP, U2A´, and Skp2 (Enkhbayar et al., 2003; Kobe and Kajava, 2001). The LRR domains in these proteins all adopt a horseshoe shape with a parallel β-sheet on the inner (concave) face, and with various secondary structures, such as α-helix, β-turn, and pII, on the outer (convex) face (Enkhbayar et al., 2003). RI interacts with the ligand ribonuclease A and angiogenin through many residues that lie on the β strands and the adjacent β-α loops, but the individual residues important for the interactions with ribonuclease A and angiogenin are different (Chen and Shapiro, 1997). For yeast RanGAP, the β-α loops and the concave face consisting of β-sheets are also likely protein interaction surfaces (Kobe and Kajava, 2001). Although structural information on how LRRs recognize their binding partners is still limited, available data suggest that the curved and elongated structure of LRR provides an ideal platform for diverse protein-protein interactions.

An envelope consisting of a two-membrane system surrounds all types of plastids. The chloroplast envelope is particularly involved in the biosynthesis of glycerolipids, chlorophylls, carotenoids, and prenylquinones (Ephritikhine et al., 2004). Comprehensive proteomics studies of *Arabidopsis* chloroplast envelope membranes identified diverse proteins that are involved in ion and metabolite transport, protein import machinery, chloroplast lipid metabolism, and vitamin and pigment biosynthesis (Ferro et al., 2003; Rolland et al., 2003). Some soluble proteins were found to be associated with the envelope membrane, including oxyradical scavengers and antioxidant enzymes, proteases, and proteins involved in carbon metabolism. The identified proteins in diverse functional categories had 0 to 14 transmembrane domains. However, the functions of one-third of the identified proteins are still unknown (Ferro et al., 2003), and their localizations in the chloroplast envelope have not been confirmed. In this study, we characterized the localization and the physiological functions of a chloroplast envelope protein, NbCEP1, in *N. benthamiana*.

[1]Department of Biology, Yonsei University, Seoul 120-749, Korea, [2]Department of Integrative Bioscience and Biotechnology, Pohang University of Science and Technology, Pohang 790-784, Korea, [3]Present address: Department of Microbiology, College of Medicine, Yonsei University, Seoul 120-752, Korea
*Correspondence: hspai@yonsei.ac.kr

Received September 15, 2009; revised October 20, 2009; accepted October 21, 2009; published online December 10, 2009

Keywords: chloroplast development, chloroplast envelope, light-induced gene expression, LRR, virus-induced gene silencing

MATERIALS AND METHODS

Virus-induced gene silencing (VIGS)

The cDNA fragments of *NbCEP1* were amplified by PCR and cloned into the *Bam*HI and *Apa*I sites of the pTV00 vector containing part of the TRV genome (Ratcliff et al., 2001). VIGS was performed as previously described (Cho et al., 2004; Kim et al., 2006; Ratcliff et al., 2001). The fourth leaf above the infiltrated leaf was used for RT-PCR and cytological analyses.

Reverse transcription (RT)-PCR

Semiquantitative RT-PCR was performed with RNA isolated from yellow sectors of the fourth leaf above the infiltrated leaf as described (Ahn et al., 2008; Park et al., 2009). Twenty micrograms of total RNA was used. Fifteen to thirty-five cycles of PCR were performed, and the appropriate number of cycles was determined empirically for each template-primer pair so that amplification was in the exponential range and did not reach a plateau. *NbCEP1* transcripts were detected using the following primer sets: NbCEP1-1 (5′-ggatccatgggctcagcttctaca-3′ and 5′-gggcccagcttgtgattccttgta-3′); NbCEP1-2 (5′-ggatccagcaaatctactgaaggag-3′ and 5′-gggcccctccaatagcatttccag-3′); and NbCEP1-3 (5′-ggatcccattggaccagagggcgc-3′ and 5′-gggcccgaacataacagcaagctcc-3′).

Subcellular localization of NbCEP1

NbCEP1 cDNAs corresponding to the full length coding region and the N-terminal transit peptide were cloned into the *Bam*HI site of the 326-GFP (green fluorescent protein) plasmid (Cho et al., 2004) to generate the NbCEP1:GFP and TP:GFP fusion proteins. The GFP fusion constructs were introduced into protoplasts prepared from *N. benthamiana* and Arabidopsis seedlings by polyethylene glycol-mediated transformation (Kim et al., 2006). Separately, NbCEP1:GFP and OEP7:RFP, as a marker for the chloroplast envelope, were co-transformed into protoplasts prepared from *Arabidopsis* seedlings. Expression of the GFP and RFP fusion constructs was monitored 24 h after transformation by confocal laser scanning microscopy, as described (Cho et al., 2004).

Protein preparation and Western blot analysis

To prepare cell extracts from protoplasts, transformed protoplasts were subjected to repeated freeze/thaw cycles in lysis buffer (150 mM NaCl, 20 mM Tris-Cl, pH 7.5, 1 mM EDTA, 1 mM EGTA, 3 mM $MgCl_2$, 0.1 mg ml^{-1} antipain, 2 mg ml^{-1} aprotinins, 0.1 mg ml^{-1} E-64, 0.1 mg ml^{-1} leupeptin, 10 mg ml^{-1} pepstatin, and 1 mM phenylmethylsulfonyl fluoride) and then centrifuged at 7,000 × *g* at 4°C for 5 min in a microfuge (Jin et al., 2001). Western blot analysis was performed using an anti-GFP antibody (Clontech, USA) as previously described (Jin et al., 2001).

Confocal laser scanning microscopy

MitoTracker Green FM (Molecular Probes) and TMRM staining of protoplasts was performed as previously described (Ahn et al., 2008; Cho et al., 2004; Tse et al., 2009).

Measurement of chlorophyll and carotenoid contents

Yellow sectors of the fourth leaf above the infiltrated leaf were collected from VIGS plants and boiled in 95% ethanol at 80°C for 30 min to extract chlorophyll. Carotenoid and chlorophyll concentrations per unit fresh weight were calculated as described (Lichtenthaler, 1987).

Measurement of *in vivo* H_2O_2

For *in vivo* H_2O_2 measurement, protoplasts isolated from the leaves of VIGS lines were incubated in 2 μM 2′,7′,-dichlorodihydrofluorescein diacetate (H_2DCFDA, Molecular Probes, USA) for 1-2 min. Protoplasts were transferred to wells on microscope slides and observed with a confocal microscope (Carl Zeiss LSM 510) with optical filters (488 nm excitation, 505 nm emission) to visualize green fluorescence of the H_2O_2 oxidized probe. Quantitative images were captured and data were analyzed using the LSM 510 image analysis software (version 2.8).

Cytological analyses

Tissue sectioning and transmission electron microscopy were carried out as described (Ahn et al., 2004) using yellow sectors of the fourth leaf above the infiltrated leaf for the VIGS lines. Plant tissues were sequentially fixed with 2.5% (v/v) glutaraldehyde and 1% osmium tetraoxide, dehydrated through an ethanol series, and embedded in Spurr's resin (EM sciences, USA). Thin sections were then made with an LKB III ultramicrotome and stained sequentially with 5% uranyl acetate and 3% lead citrate, followed by observation by transmission electron microscopy (model JEOL 1200 EXII, JEOL, Japan).

RESULTS AND DISCUSSION

Identification of NbCEP1

For functional genomics using VIGS, > 2,900 individual cDNAs were selected from ~15,000 *N. benthamiana* ESTs and cloned into the pTV00 vector. The partial *NbCEP1* cDNA used in the initial VIGS screening was ~1.1 kb in length. The full-length *NbCEP1* cDNA was obtained by 5′-RACE (Rapid Amplification of cDNA Ends) PCR using cDNAs synthesized from *N. benthamiana* seedling RNA. *NbCEP1* encodes a polypeptide of 614 amino acids, corresponding to a theoretical molecular mass of 66,107.25 Da. As shown in Fig. 1A, the NbCEP1 protein contains an N-terminal chloroplast transit peptide (residues 1-88), a transmembrane domain (residues 98-120), and 15 leucine-rich-repeats (LRRs; residues 178-601). The amino acid sequence of *N. benthamiana NbCEP1* was aligned with related sequences from *Arabidopsis thaliana*, tomato (*Lycopersicon esculentum*), and castor bean (*Ricinus communis*) (Fig. 1B), which indicated that the *CEP1* gene is well conserved among diverse plant species. *CEP1* is a single copy gene in *Arabidopsis* (At1g10510), and *Arabidopsis* CEP1 was identified as a putative chloroplast envelope protein based on a proteomics approach (Ferro et al., 2003). *Arabidopsis* CEP1 mutants exhibit an embryonic lethal phenotype at the globular stage (emb2004) according to the SeedGenes Project database (http://www.seedgenes.org/) to identify embryonic lethal genes in Arabidopsis. Figure 1C shows the sequence alignment of the 15 LRRs from NbCEP1 in comparison with the conserved residues of the LRR motif. The LRR structural motif is composed of repeating 20-29 amino acid stretches that contain many leucines. The LRR motif has been found in many functionally unrelated proteins with repeat numbers ranging from 2 to 45, and the primary function of LRRs is apparently to provide a structural framework for protein-protein interactions (Kobe and Kajava, 2001). The predicted structure of the NbCEP1 LRRs according to the SWISS MODEL (an automated comparative protein modeling program; Arnold et al., 2006; http://swissmodel.expasy.org/) is shown in Fig. 1D. The NbCEP1 LRR structure most closely resembles the LRR structure of a porcine ribonuclease inhibitor, in which each repeat has a β sheet-turn-α helix structure, and many repeats are assembled into a horseshoe shape with interior parallel β sheets and an exterior array of α helices (Kobe and Deisenhofer, 1994; Kobe and Kajava, 2001).

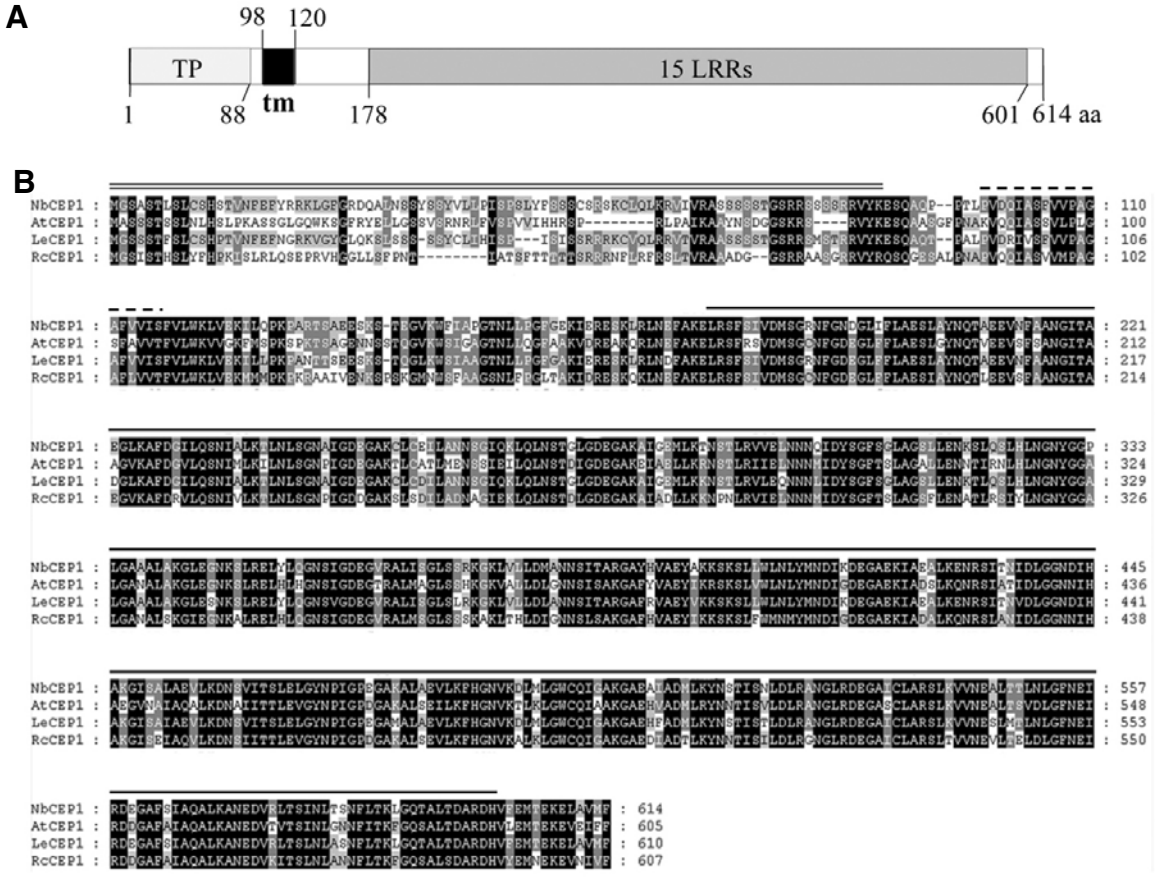

Fig. 1. Protein structure and sequence alignment of NbCEP1. (A) Schematic of the NbCEP1 protein with the chloroplast transit peptide (TP), a transmembrane domain (tm), and the 15 leucine-rich-repeats (LRRs). (B) Alignment of *Nicotiana benthamiana* NbCEP1 with related sequences from other species. The protein sequences of NbCEP1 and its homologs from *Arabidopsis* (AtCEP1), tomato (LeCEP1), and castor-bean (RcCEP1) are aligned. The residues that are conserved between the compared sequences are shaded in black or light gray based on the degree of conservation. The *thick overline* indicates the chloroplast transit peptide, and the *dashed overline* indicates the transmembrane domain. The *thin overline* indicates the 15 LRRs. The GenBank accession numbers for the proteins in the alignment are as follows: NbCEP1, GQ477179; LeCEP1, AK320873; AtCEP1, AY091215; RcCEP1, XM_002520172. (C) Sequence alignment of the 15 LRRs of NbCEP1. The conserved residues of the LRR motif of the RI type based on Kobe and Kajava (2001) are shown (*Con.*). Residues identical or conservatively substituted in more than 50% and 30% of the repeats are shown in *uppercase* and *lowercase*, respectively. N*, N (Asn) or C (Cys) residue; *o*, a nonpolar residue; *x*, any residue; '-', possible insertion site. (D) A predicted structure of NbCEP1 LRRs (residues numbers 178-601) according to the SWISS MODEL (an automated comparative protein modeling program; http://swissmodel.expasy.org/).

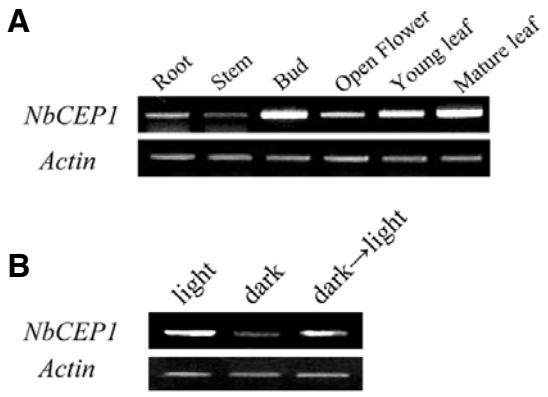

Fig. 2. Gene expression of *NbCEP1*. (A) Expression of *NbCEP1* in various plant tissues. Semiquantitative RT-PCR analysis was performed with total RNA from *N. benthamiana* plant tissues using *NbCEP1*-specific primers. The transcript level of actin was measured as a control. (B) Expression of *NbCEP1* in response to light. *N. benthamiana* seedlings were grown for 7 d under normal light conditions (16 h light/8 h dark) (*light*), under dark conditions (*dark*), or under dark conditions followed by a transfer to light for 1 h (*dark* → *light*) prior to semiquantitative RT-PCR analysis of *NbCEP1* expression.

Expression patterns of *NbCEP1*

Semiquantitative RT-PCR analysis was performed using *NbCEP1*-specific primer sets. RT-PCR products of *NbCEP1* were detected in all *N. benthamiana* tissues examined, including roots, stems, flower buds, open flowers, young leaves, and mature leaves, and the highest levels of transcripts were found in mature leaves and flower buds (Fig. 2A). Thus, NbCEP1 is expressed in both photosynthetic and nonphotosynthetic tissues. *NbCEP1* gene expression was stimulated by light (Fig. 2B). *N. benthamiana* seedlings were grown on MS medium for a week under normal light conditions (16 h light/8 h dark), under dark conditions, or under dark conditions followed by transfer to light for 1 h. The *NbCEP1* mRNA level was lower in dark-grown seedlings than in light-grown seedlings, but exposure to light for 1 h after growth in the dark increased the *NbCEP1* mRNA level to that of light-grown seedlings (Fig. 2B).

Localization of NbCEP1 in the chloroplast envelope

NbCEP1 contains a long N-terminal extension that exhibits characteristic features of a chloroplast transit peptide (Bruce, 2000; Jarvis, 2008). Proteomics of *Arabidopsis* chloroplast envelope membranes identified CEP1 as a putative envelope protein with no known function, but further experiments were not carried out (Ferro et al., 2003). To investigate the subcellular localization of NbCEP1, we generated fusion proteins in which the full length

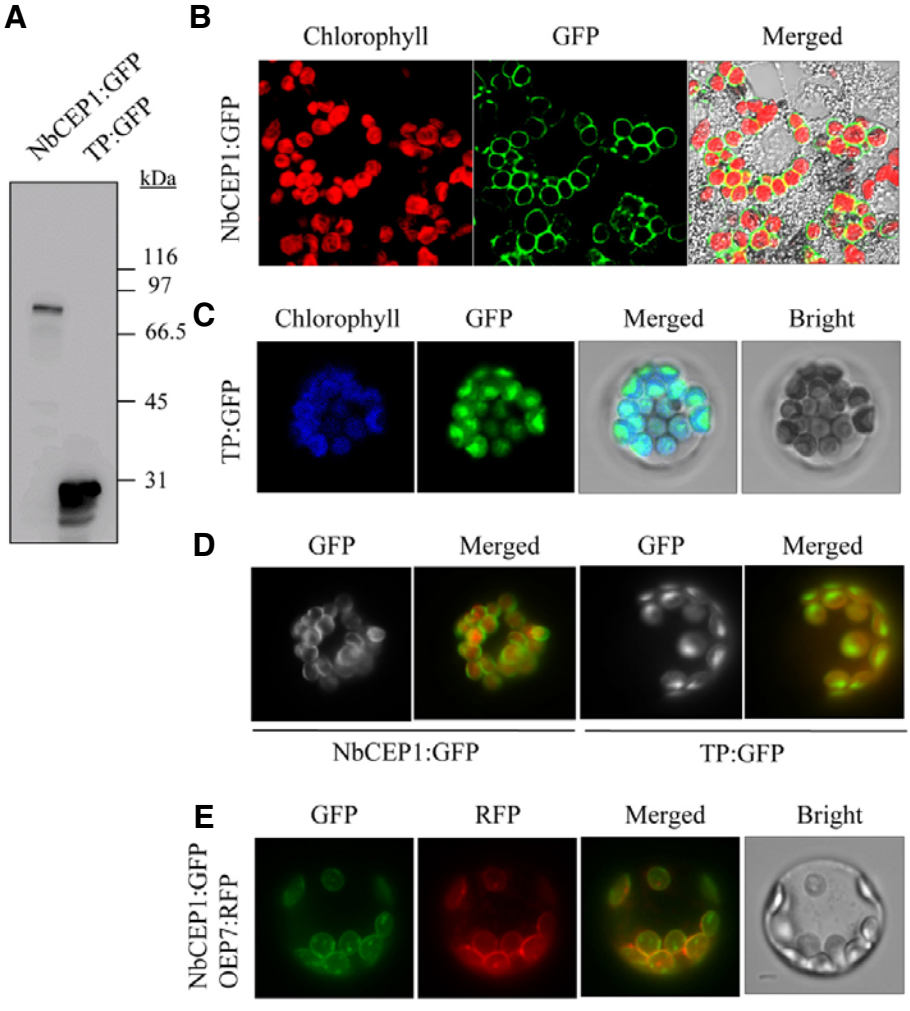

Fig. 3. Subcellular localization of NbCEP1. (A) GFP fusion constructs of the full-length NbCEP1 and the N-terminal chloroplast transit peptide of NbCEP1 are termed NbCEP1: GFP and TP:GFP, respectively. Protein extracts prepared from *N. benthamiana* protoplasts transformed with *NbCEP1:GFP* or *TP:GFP* were analyzed by Western blotting using an anti-GFP antibody. (B) The localization of the fluorescent signal in NbCEP1:GFP-transformed *N. benthamiana* protoplasts was examined 24 h after transformation by confocal laser scanning microscopy. Chlorophyll autofluorescence and a merged image are also shown. (C) The localization of the fluorescent signal in TP:GFP-transformed *N. benthamiana* protoplasts was examined. Chlorophyll autofluorescence, merged, and bright-field images are also shown. (D) The localization of the fluorescent signal in NbCEP1:GFP- or TP:GFP-transformed Arabidopsis protoplasts was examined. (E) *Arabidopsis* protoplasts were co-transformed with *NbCEP1:GFP* and *OEP7:RFP* as a marker for the chloroplast envelope (Schleiff et al., 2001), and localization of fluorescent signals was examined. GFP, RFP, merged and bright-field images are shown.

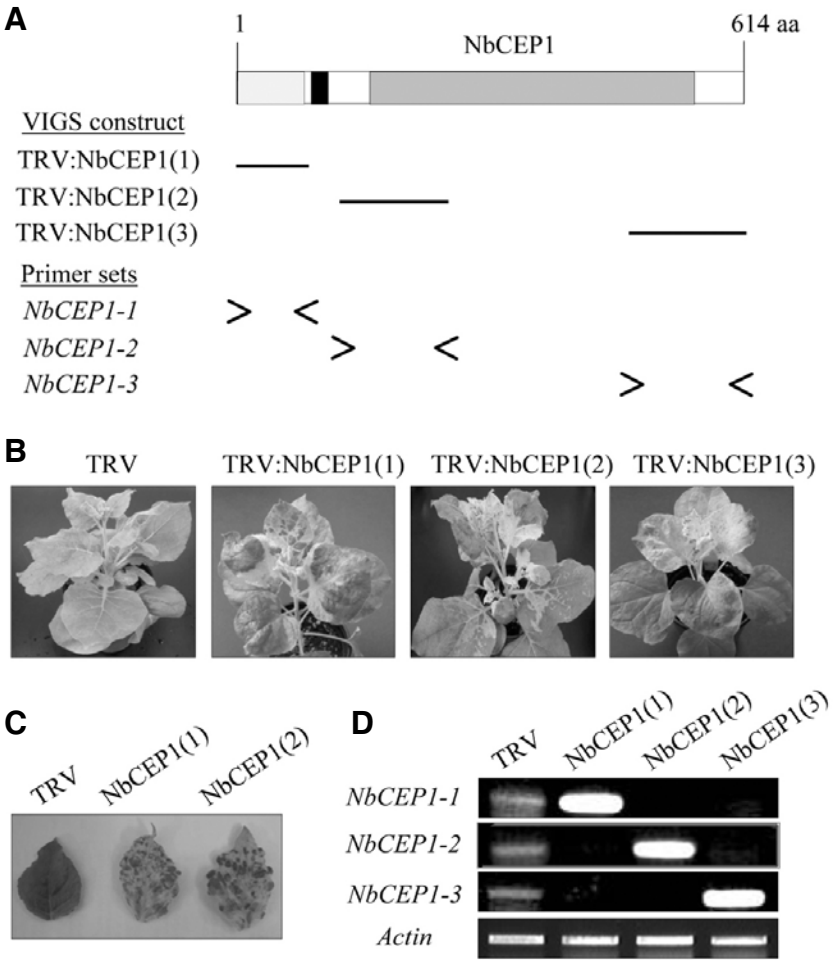

Fig. 4. VIGS phenotypes and suppression of endogenous transcripts. (A) Schematic representation of the structure of the *NbCEP1* protein-coding region. The three VIGS constructs containing different regions of the *NbCEP1* cDNA are marked by bars. *N. benthamiana* plants were infected with *Agrobacterium* containing the TRV control or one of the TRV:NbCEP1 constructs. The positions of the primer sets used for RT-PCR analyses (NbCEP1-1, NbCEP1-2, and NbCEP1-3) are shown. (B, C) Phenotypes of the three TRV:NbCEP1 VIGS lines (B) and leaf morphology (C). The plants were photographed 20 d post-inoculation. (D) Semiquantitative RT-PCR analysis of *NbCEP1* transcript levels. RNA was extracted from the leaves of each VIGS line. The NbCEP1-1, NbCEP1-2, and NbCEP1-3 primer sets were used for RT-PCR analysis, and actin mRNA levels were measured as a control.

NbCEP1 or its transit peptide was fused to GFP (26.9 kDa) under the control of the CaMV35S promoter to generate NbCEP1:GFP and TP:GFP, respectively. The DNA constructs encoding the different GFP fusion proteins were introduced into protoplasts isolated from *N. benthamiana* seedlings, and gene expression was examined by Western blot analysis with an anti-GFP antibody. Protein bands of ~85 and ~27 kDa, which are consistent with expected protein sizes after removal of the chloroplast transit peptides, were detected in NbCEP1:GFP- and TP:GFP-transformed protoplasts, respectively, indicating that the GFP-fusion proteins were processed during import into chloroplasts (Fig. 3A). Based on confocal laser scanning microscopy, the NbCEP1:GFP signal was mainly localized in the chloroplast envelope (Fig. 3B). The TP:GFP signal was observed within chloroplasts, but it did not significantly overlap with chlorophyll autofluorescence, indicating that the expressed protein is mostly localized in the stroma (Fig. 3C). When we transformed the NbCEP1:GFP and TP: GFP constructs into Arabidopsis protoplasts, we obtained the similar results (Fig. 3D). The NbCEP1:GFP and TP:GFP signals were mainly detected in the envelope and in the stroma, respectively (Fig. 3D). To confirm the envelope localization of NbCEP1, we co-transformed NbCEP1:GFP and OEP7:RFP, a marker protein for chloroplast envelope targeting (Schleiff et al., 2001), into *Arabidopsis* protoplasts, followed by confocal laser scanning microscopy (Fig. 3E). The green fluorescent signal of NbCEP1:GFP co-localized with the red fluorescent signal of OEP7:RFP, indicating chloroplast envelope localization of NbCEP1 (Fig. 3E).

Suppression of *NbCEP1* expression by VIGS

Three different *NbCEP1* cDNA fragments were cloned into the TRV-based VIGS vector pTV00 (Ratcliff et al., 2001), and *N. benthamiana* plants were infiltrated with *Agrobacterium* containing each plasmid (Fig. 4A). TRV:NbCEP1(1), TRV:NbCEP1(2), and TRV:NbCEP1(3) contain 270 bp, 400 bp, and 430 bp of the *NbCEP1* cDNA, respectively. VIGS with these constructs resulted in a yellowing phenotype in newly emerged leaves, and there were no phenotypic differences in yellowing patterns between the three lines (Figs. 4B and 4C). The overall growth of the VIGS plants was normal. This yellowing phenotype has been observed in all of the *N. benthamiana* plants (n > 120) that have been subjected to *NbCEP1* VIGS to date.

The effects of gene silencing on the levels of endogenous *NbCEP1* mRNA were examined by semiquantitative RT-PCR (Fig. 4D). RT-PCR using the NbCEP1-1 primers (indicated in Fig. 4A) produced significantly reduced levels of PCR products in the yellow sectors of leaves from the TRV:NbCEP1(2) and TRV:NbCEP1(3) lines, indicating that the endogenous level of *NbCEP1* transcripts is greatly reduced in these plants (Fig. 4D). The same primers detected high levels of viral genomic transcripts in the TRV:NbCEP1(1) line. Similarly, RT-PCR using the NbCEP1-2 and NbCEP1-3 primers produced significantly reduced amounts of PCR products in the yellow sectors of leaves from the TRV:NbCEP1(1) and TRV:NbCEP1(3), and TRV:

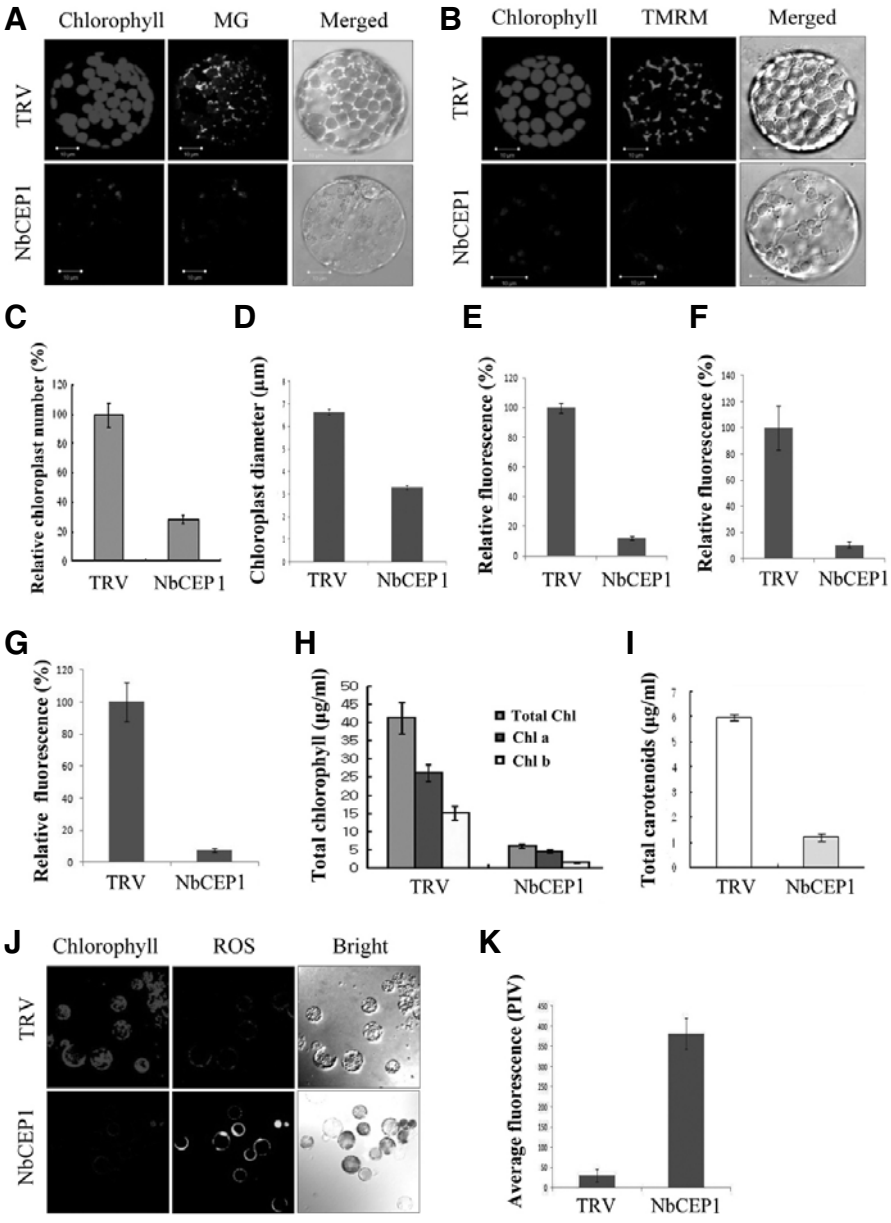

Fig. 5. Chloroplast and mitochondrial abnormalities. The three replicate experiments resulted in very similar data. (A, B) Confocal laser scanning microscopy of chloroplasts and mitochondria in protoplasts isolated from the fourth leaf above the infiltrated leaf in the TRV and TRV:NbCEP1 VIGS lines. Chloroplasts were visualized by chlorophyll autofluorescence. Mitochondria were visualized by staining with TMRM and MitoTracker Green FM (MG). Scale bars = 5 μm. (C) Determination of the number of chloroplasts per protoplast by confocal microscopy. TRV controls had an average of 58 chloroplasts per protoplast. The data points represent means ± SD of 30 individual protoplasts. (D) The average diameter of chloroplasts from TRV and TRV:NbCEP1 VIGS lines. The average diameter of TRV control chloroplasts was ~6.7 μm. The data points represent means ± SD of 30 individual protoplasts. (E-G) The relative fluorescence of chlorophyll autofluorescence (E), TMRM (F), and MitoTracker Green FM (G) in individual protoplasts was quantified by confocal microscopy. Data points represent means ± SD of 20-30 individual protoplasts. (H) Quantification of the levels of total chlorophyll, chlorophyll a, and chlorophyll b in TRV and TRV:NbCEP1 leaves. (I) Quantification of the levels of total carotenoids in TRV and TRV:NbCEP1 leaves. (J, K) ROS production. Leaf protoplasts were incubated in 2 μM H_2DCFDA for 90 s (J). H_2DCFDA is a ROS indicator that becomes fluorescent when oxidized by ROS within the cell. The fluorescence of TRV and TRV:NbCEP1 protoplasts was quantified by pixel intensity (K). Data points represent means ± SD of 20-30 individual protoplasts. PIV, pixel intensity values.

NbCEP1(1) and TRV:NbCEP1(2) lines, respectively, while the same primers detected high levels of viral genomic transcripts in the TRV:NbCEP1(2) and TRV:NbCEP1(3) lines, respectively. The transcript level of actin remained constant (Fig. 4D).

Chloroplast abnormalities in NbCEP1 VIGS lines

Protoplasts were prepared from TRV control leaves and the yellow sectors of leaves from TRV:NbCEP1 plants, and examined by confocal laser scanning microscopy (Figs. 5A and 5B). The average chloroplast numbers in TRV:NbCEP1 protoplasts were only ~20.2% of that of the TRV control (Fig. 5C). Furthermore, chloroplasts from the TRV:NbCEP1 line were smaller than those from TRV controls, measuring ~47.8% of the average control diameter (corresponding to ~10.9% of the volume) (Fig. 5D). Consistent with the observed chloroplast defects, chlorophyll autofluorescence in *NbCEP1*-silenced protoplasts was ~12.2% of that of TRV controls (Fig. 5E). Total chlorophyll and carotenoid levels in the yellow sectors of the TRV:NbCEP1 leaves were reduced to approximately ~14.7% and ~20.3% of that in the TRV control, respectively, suggesting defective biosynthesis of photosynthetic pigments in NbCEP1-depleted chloroplasts (Figs. 5H and 5I). Mitochondria in leaf protoplasts from the TRV control and TRV:NbCEP1 lines were examined with TMRM and MitoTracker Green FM (MG) fluorescent probes (Figs. 5F and 5G). TMRM indicates mitochondrial membrane potential: decreased membrane potential leads to a decrease in fluorescence (Zhang et al., 2001). The average TMRM fluorescence of TRV:NbCEP1 protoplasts was about ~8.4% of the fluorescence of the TRV control, indicating reduced mitochondrial membrane potential or reduced mitochondrial numbers in the protoplasts (Fig. 5F). MitoTracker Green FM (MG) is an indicator of mitochondrial mass, which accumu-

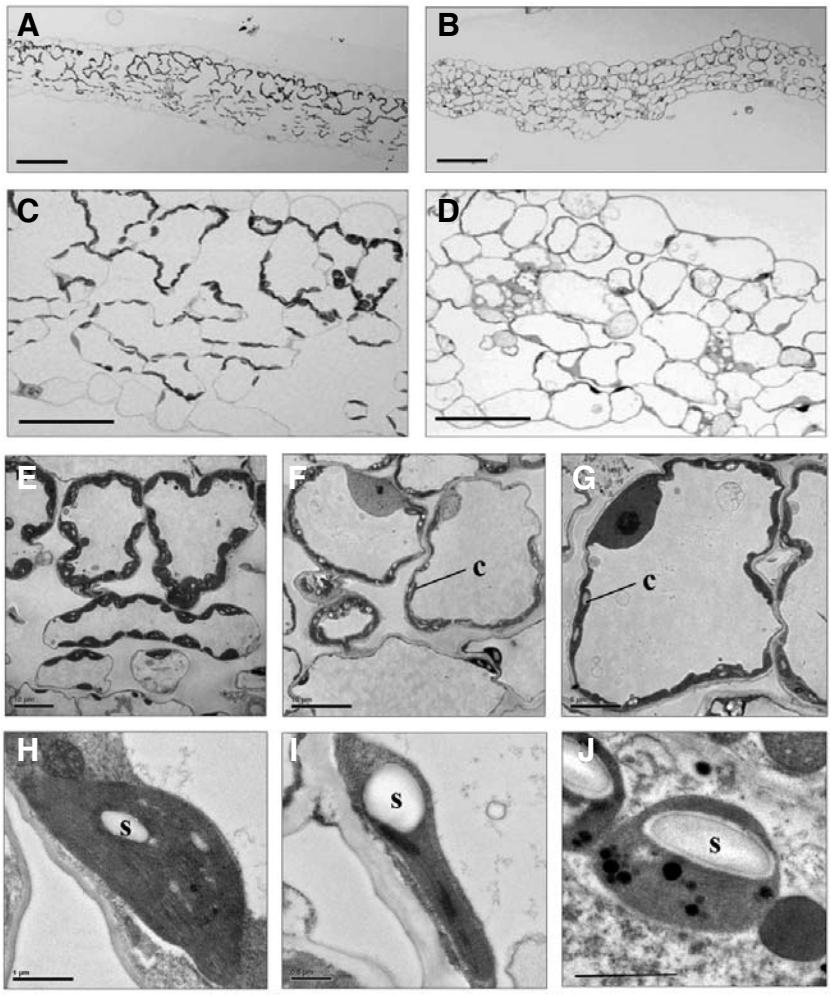

Fig. 6. Ultrastructure of mesophyll cell chloroplasts. (A, B) Light micrographs of leaf transverse sections from TRV (A) and TRV: NbCEP1 (B) plants. Scale bars = 100 μm. (C-J) Transmission electron micrographs of leaf transverse sections (C, D), leaf mesophyll cells (E-G), and chloroplasts (H-J) from the TRV control (C, E, and H) and TRV:NbCEP1 lines (D, F, G, I and J). *c*, chloroplast; *s*, starch. Scale bars = 50 μm in C, D; 10 μm in E, F; 5 μm in G; 1 μm in H, J; 0.5 μm in I.

lates in mitochondria regardless of the mitochondrial membrane potential (Oubrahim et al., 2001). The MG fluorescence of TRV:NbCEP1 protoplasts was also lower than that of the TRV control, about ~7.7%, indicating that mitochondrial numbers and/or mass were reduced in the NbCEP1 VIGS lines (Fig. 5G). To assess production of reactive oxygen species (ROS; Ahmad et al., 2008), leaf protoplasts from TRV and TRV:NbCEP1 lines were incubated with H_2DCFDA, which is a cell-permanent indicator for ROS that produces a green fluorescent signal when chemically modified by H_2O_2 (Figs. 5J and 5K). The accumulation of fluorescent H_2DCFDA in protoplasts from the TRV: NbCEP1 line was ~15-fold higher than that of the TRV control, indicating excessive production of ROS (Fig. 5K). In plants under illumination, reactive oxygen species (ROS) are mainly produced from the photosynthetic electron transport chain (Ivanov and Khorobrykh, 2003). Impaired electron donation to photosystem II causes detachment of electrons and organic radical generation by P680, leading to hydroperoxide formation by reacting with oxygen (Ivanov and Khorobrykh, 2003). Thus the formation of excess ROS in a cell is one consequence of chloroplast dysfunction. These results demonstrate that NbCEP1 deficiency results in defective biogenesis of both chloroplasts and mitochondria. The mitochondrial abnormalities are likely the indirect consequences of cellular stress caused by perturbed chloroplast functions, which is correlated with excessive ROS formation in the NbCEP1-deficient cells.

Ultrastructural analysis of chloroplasts

Transverse leaf sections revealed that the TRV control leaves had the typical leaf structure of dicotyledonous plants, with distinct adaxial and abaxial epidermal layers, and both the palisade and spongy mesophyll layer had densely stained chloroplasts (Figs. 6A, 6C, and 6E). Transmission electron microscopy of transverse leaf sections also revealed that mesophyll cell chloroplasts of the TRV control had a well-developed thylakoid membrane system (Fig. 6H). In the yellow sector of TRV:NbCEP1 leaves, the typical organization of the palisade and spongy mesophyll cells was mostly maintained, although the cells were more spherical and the chloroplasts were not readily visible (Figs. 6B and 6D). Reduced numbers and morphological abnormalities of the chloroplast were apparent in a TRV:NbCEP1 mesophyll cell (Figs. 6F and 6G). The affected chloroplasts were small and irregular in shape, and contained poorly developed thylakoids (Figs. 6I and 6J).

In this study, we showed that NbCEP1 is mainly localized in the chloroplast envelope, consistent with the identification of *Arabidopsis* CEP1 as a putative envelope protein using a proteomics approach (Ferro et al., 2003). Depletion of NbCEP1 using VIGS causes severe defects in chloroplast development in *N. benthamiana*. Specifically, the chloroplast number and their sizes were significantly reduced, compared with that of the TRV control. The abnormal chloroplasts lacked fully developed thylakoid membranes, and the levels of chlorophylls and caro-

tenoids were much reduced. Since NbCEP1 mostly consists of LRRs, the protein interactions mediated by these motifs likely play a key role in NbCEP1 functions. The assembled structure of the 15 LRRs of NbCEP1 is very similar to that of a porcine ribonuclease inhibitor (RI) that also has 15 LRRs, indicating the possibility that NbCEP1 is an ribonuclease inhibitor (Kobe and Kajava, 2001). However, purified recombinant NbCEP1 proteins showed no inhibitory activities against various ribonucleases, suggesting that NbCEP1 and RI have no functional relationship (data not shown). Furthermore, NbCEP1 deficiency did not affect the chloroplast targeting of several chloroplast marker proteins, excluding the possibility of its involvement in protein import (data not shown). To identify NbCEP1-interacting proteins, we carried out a LexA-based yeast two-hybrid screen with the LRR domain of NbCEP1 as bait and, so far, we have not found true NbCEP1 partners among the two-hybrid-positive clones we obtained (data not shown). The N-terminal transmembrane domain in NbCEP1 indicates that the interaction between NbCEP1 and its partner(s) may occur near chloroplast envelope membranes. Thus, other methods that specifically detect membrane-proximal protein interactions may be required to find NbCEP1-interacting proteins.

Arabidopsis knockout mutations of CEP1 result in embryonic lethality around the globular stage (emb2004; http://www.seedgenes.org/), indicating that CEP1 is essential for normal embryogenesis. Previously, knockout mutations affecting chloroplast proteins of diverse functions, such as Toc34, pentatricopeptide proteins, a glycyl-tRNA synthetase, and DNA gyrase subunit A, have also been found to cause embryonic lethality (Constan et al., 2004; Cushing et al., 2005; Uwer et al., 1998; Wall et al., 2004). Thus, plastids appear to be essential for development of the embryo well before it gains photosynthetic ability, most likely for the biosynthesis of essential metabolites. As it is localized in the plastid envelope, CEP1 may regulate a critical, as-yet unidentified, process that is required for embryo development. We observed that NbCEP1 depletion by VIGS severely affects chloroplast development, but that it does not significantly affect overall plant growth. Considering the embryonic-lethal phenotype of *Arabidopsis cep1* mutants, this VIGS phenotype is rather mild. This discrepancy may be caused by the fact that VIGS seldom results in 100% gene silencing. Alternatively, it is also possible that the CEP1 function is essential for the embryonic stage, but not for the plant adult stage. Deciphering the molecular nature of NbCEP1 interactions is required for understanding the mechanisms of NbCEP1 function in chloroplasts.

ACKNOWLEDGMENTS

This research was supported by grants from the Plant Diversity Research Center of the 21st Century Frontier Research Program, the BioGreen21 Program (Rural Development Administration, Korea), and the Plant Signaling Network Research Center (at Korea University) of the Science Research Center Program, all of which are funded by the Ministry of Science and Technology of Korea.

REFERENCES

Ahmad, P., Sarwat, M., and Sharma, S. (2008). Reactive oxygen species, antioxidants and signaling in plants. J. Plant Biol. *51*, 167-173.

Ahn, J.W., Kim, M., Kim, G.T., Lim, J.H., and Pai, H.-S. (2004). Phytocalpain controls the proliferation and differentiation fates of cells in plant organ development. Plant J. *38*, 969-981.

Ahn, C.S., and Pai, H.-S. (2008). Physiological function of IspE, a plastid MEP pathway gene for isoprenoid biosynthesis, in organelle biogenesis and cell morphogenesis in *Nicotiana benthamiana*. Plant Mol. Biol. *66,* 503-517.

Arnold, K., Bordoli, L., Kopp, J., and Schwede, T. (2006). The SWISS-MODEL Workspace: A web-based environment for protein structure homology modelling. Bioinformatics *22,* 195-201.

Bruce, D.B. (2000). Chloroplast transit peptides: structure, function and evolution. Trends Cell Biol. *10,* 440-447.

Chen, C.Z., and Shapiro, R. (1997). Site-specific mutagenesis reveals differences in the structural bases for tight binding of RNase inhibitor to angiogenin and RNase A. Proc. Natl. Acad. Sci. USA *94,* 1761-1766.

Cho, H.S., Lee, S.S., Kim, K.D., Kim, S.J., Hwang, I., Lim, J.S., Park, Y.I., and Pai, H.-S. (2004). DNA gyrase is involved in chloroplast nucleoid partitioning. Plant Cell *16*, 2665-2682.

Constan, D., Patel, R., Keegstra, K., and Jarvis, P. (2004). An outer envelope membrane component of the plastid protein import apparatus plays an essential role in Arabidopsis. Plant J. *38,* 93-106.

Cushing, D.A., Forsthoefel, N.R., Gestaut, D.R., and Vernon, D.M. (2005). Arabidopsis emb175 and other *ppr* knockout mutants reveal essential roles for pentatricopeptide repeat (PPR) proteins in plant embryogenesis. Planta *221,* 424-436.

Enkhbayar, P., Kamiya, M., Osaki, M., Matsumoto, T., and Matsushima, N. (2004). Structural principles of leucine-rich repeat (LRR) proteins. Proteins *54*, 394-403.

Ephritikhine, G., Ferro, M., and Rolland, N. (2004). Plant membrane proteomics. Plant Physiol. Biochem. *42,* 943-962.

Ferro, M., Salvi, D., Brugière, S., Miras, S., Kowalski, S., Louwagie, M., Garin, J., Joyard, J., and Rolland, N. (2003). Proteomics of the chloroplast envelope membranes from *Arabidopsis thaliana*. Mol. Cell Proteomics *2,* 325-345.

Ivanov, B., and Khorobrykh, S. (2003). Participation of photosynthetic electron transport in production and scavenging of reactive oxygen species. Antioxid Redox Signal. *5*, 43-53.

Jarvis, P. (2008) Targeting of nucleus-encoded proteins to chloroplasts in plants. New Phytol. *179,* 257-285.

Jin, J.B., Kim, Y.A., Kim, S.J., Lee, S.H., Kim, D.H., Cheong, G.W. and Hwang, I. (2001). A new dynamin-like protein, ADL6, is involved in trafficking from the trans-Golgi network to the central vacuole in Arabidopsis. Plant Cell *13*, 1511-1526.

Kim, M., Ahn, J.W., Jin, U.H., Choi, D., Paek, K.H., and Pai, H.-S. (2003). Activation of the programmed cell death pathway by inhibition of proteasome function in plants. J. Biol. Chem. *278,* 19406-19415.

Kim, M., Lim, J.-H., Ahn, C.S., Park, K., Kim, G.T., Kim, W.T., and Pai, H.-S. (2006). Mitochondria-associated hexokinases play a role in the control of programmed cell death in *Nicotiana benthamiana*. Plant Cell *18*, 2341-2355.

Kobe, B., and Deisenhofer, J. (1994). The leucine-rich repeat: a versatile binding motif. Trends Biochem. Sci. *19,* 415-421.

Kobe, B., and Kajava, A.V. (2001). The leucine-rich repeat as a protein recognition motif. Curr. Opin. Struct. Biol. *11,* 725-732.

Lichtenthaler, H.K. (1987). Chlorophylls and carotenoids: Pigments of photosynthetic biomembranes. Methods Enzymol. *148,* 350-382.

Oubrahim, H., Stadtman, E.R., and Chock, P.B. (2001). Mitochondria play no roles in Mn(II)-induced apoptosis in HeLa cells. Proc. Natl. Acad. Sci. USA *98,* 9505-9510.

Park, H.C., Kim, M.L., Kang, Y.H., Jeong, J.C., Cheong, M.S., Choi, W., Lee, S.Y., Cho, M.C., Chung, W.S., and Yun, D.J. (2009). Functional analysis of the stress-inducible soybean calmodulin isoform-4 (GmCaM-4) promoter in transgenic tobacco plants. Mol. Cells *27*, 475-480.

Ratcliff, F., Martin-Hernandez, A.M., and Baulcombe, D.C. (2001). Tobacco rattle virus as a vector for analysis of gene function by silencing. Plant J. *25*, 237-245.

Rolland, N., Ferro, M., Seigneurin-Berny, D., Garin, J., Douce, R., and Joyard, J. (2003). Proteomics of chloroplast envelope membranes. Photosynth. Res. *78,* 205-230.

Schleiff, E., Tien, R., Salomon, M., and Soll, J. (2001). Lipid composition of outer leaflet of chloroplast outer envelope determines topology of OEP7. Mol. Biol. Cell *12,* 4090-4102.

Tse, Y.C., Lam, S.K., and Jiang, L. (2009) Organelle identification and characterization in plant cells: using a combinational approach of confocal immunofluorescence and electron microscope. J. Plant Biol. *52*, 1-9.

Uwer, U., Willmitzer, L., and Altmann, T. (1998). Inactivation of a glycyl-tRNA synthetase leads to an arrest in plant embryo development. Plant Cell *10,* 1277-1294.

Wall, M.K., Mitchenall, L.A., and Maxwell, A. (2004). *Arabidopsis thaliana* DNA gyrase is targeted to chloroplasts and mitochondria. Proc. Natl. Acad. Sci. USA *101,* 7821-7826.
Zhang, H., Huang, H.M., Carson, R.C., Mahmood, J., Thomas, H.M., and Gibson, G.E. (2001). Assessment of membrane potentials of mitochondrial populations in living cells. Anal. Biochem. *298,* 170-180.